**Supporting Information**

# Paper-Based Electrochemical Biosensor for Diagnosing COVID-19: Detection of SARS-CoV-2 Antibodies and Antigen

Abdulhadee Yakoh[a], Umaporn Pimpitak[a], Sirirat Rengpipat[b,c], Nattiya Hirankarn[d,e], Orawon Chailapakul[f], Sudkate Chaiyo[a,f]*

[a] Institute of Biotechnology and Genetic Engineering, Chulalongkorn University, Bangkok 10330, Thailand

[b] Department of Microbiology, Faculty of Science, Chulalongkorn University, Bangkok 10330, Thailand

[c] Qualified Diagnostic Development Center, Chulalongkorn University, Bangkok 10330, Thailand

[d] Department of Microbiology, Faculty of Medicine, Chulalongkorn University, Bangkok 10330, Thailand

[e] Center of Excellence in Immunology and Immune-mediated Diseases, Chulalongkorn University, Bangkok 10330, Thailand

[f] Electrochemistry and Optical Spectroscopy Center of Excellence (EOSCE), Department of Chemistry, Faculty of Science, Chulalongkorn University, Bangkok 10330, Thailand

Corresponding author at

E-mail address: sudkate.c@chula.ac.th (S. Chaiyo)

**Chemicals and Apparatus**

All commercial reagents were of analytical grade and handled according to the suppliers' material safety data sheets. Paste materials for electrode fabrication, including graphene (SSG-1760A) and silver/silver chloride (C2130809D5), were purchased from Serve Science Co., Ltd. (Bangkok, Thailand) and Gwent group/Sun Chemical (Pontypool, U.K.), respectively. SARS-CoV-2 spike protein (RBD) (cat no.: Z03483-100; Z03483-1), SARS-CoV-2 spike S1 IgM antibody (cat no.: A02046) and SARS-CoV-2 spike S1 IgG antibody (cat no.: A02038-1) were purchased from GenScript USA, Inc (NJ, USA). Phosphate buffer saline (PBS), 1-ethyl-3-(3-dimethylaminopropyl) carbodiimide (EDC), N-hydroxysulfosuccinimide (sulfo-NHS) and skim milk (SKI) were purchased from Sigma-Aldrich (MO, USA). Potassium nitrate was purchased from Carlo Erba (Barcelona, Spain). A water-based dispersion of single-layer graphene oxide (GO) sheets (5 mg $mL^{-1}$) with average lateral (x, y) and through-plane (z) dimension range of ≈500 and 1−1.2 nm, respectively, and a C/O ratio of about one unit (supplier's data) was purchased from Angstron Materials (OH, USA). All aqueous solutions were freshly prepared in ultrapure water produced using a Milli-Q system (>18.2 MΩ cm) purchased from Millipore. Whatman 4 chromatography paper was purchased from Fisher Scientific (PA). The wax pattern was printed with a wax printer (Xerox ColorQube model 8580, Japan). SEM characterization was performed using the JSM-7610F field emission scanning electron microscope (FESEM) (JEOL Ltd., Japan). TEM images were recorded by a H-7650 transmission electron microscope (Hitachi model, Japan). Voltammetric experiments were performed with Emstat3 Blue wireless potentiostat (PalmSens BV, Netherlands). Electrochemical impedance spectroscopy (EIS) was performed with a PalmSens 4 potentiostat/impedance analyzer (PalmSens BV, Netherlands). 3D measuring laser microscope was performed using LEXT OL55000 (Olympus, Japan).

**Electrochemical Measurements**

All electrochemical measurement was performed with 5 mM $[Fe(CN)_6]^{3-/4-}$ in 0.1 M KCl as a redox probe. The square-wave voltammetry (SWV) was monitored for both SARS-CoV-2 antibodies and SARS-CoV-2 spike protein detection. The potential was set in the range between -0.2 to 0.7 V (vs. Ag/AgCl). Also, other electrochemical parameters were set as follow; equilibration time: 120s, step potential: 0.01 V (vs. Ag/AgCl), amplitude: 0.1 V (vs. Ag/AgCl), and frequency: 20 Hz.

For electrochemical characterizations, the Nyquist diagram of EIS was recorded in the frequency range of 0.01 Hz−100 kHz with the AC potential of 0.1 V (vs. Ag/AgCl) and logarithmic scale of 10 points per decade. For cyclic voltammetry, the potential scan was set between -0.6 to 0.9 V (vs. Ag/AgCl) with potential step of 0.01 V (vs. Ag/AgCl) and scan rate of 0.1 V/s

**Preparation of AuNPs-conjugated goat anti-human antibody**

AuNPs (20 nm and 40 nm size) were first prepared following the literature (Zhang et al. 2009). It should be noted that the AuNPs with 20 nm size were used for the goat anti-human IgM conjugation, while the AuNPs with 40 nm size were used for the goat anti-human IgG conjugation. Overall conjugation procedures were applied to both goat anti-human IgM and goat anti-human IgG conjugation. Next, the pH of the AuNPs solution (100 mL) was adjusted to pH 8.2. Then, 10 mL of selected concentration of goat anti-human antibody was slowly added to the pH adjusted gold solution and stirred for 30 min. 10 mL of 10% BSA in 20 mM sodium borate buffer pH 8.2 was then added to the prepared solution and continued stirring for 10 min. The mixed solution was further centrifuged at 25000 xg (10°C) for 30 min. Lastly, the supernatant was removed, and the separated precipitation was washed (3X) and adjusted volume with 20 mM sodium borate buffer containing 0.01% thimerosal to the volume of 10 mL. The prepared AuNPs conjugated antibody was kept at 4°C before use.

**Preparation of the colorimetric LFA device.**

The colorimetric LFA device consists of 4 parts; a sample pad, a conjugate pad, a nitrocellulose membrane, and an absorbent pad, assembled on a plastic backing card. The schematic illustration of the LFA device is presented in **Figure 4A**. Each LFA strip was fabricated for each antibody (IgG and IgM). The sample pad was initially treated with 1%BSA mixed with 0.5% tween20, while a conjugate pad was pretreated with 3% sucrose. Here, gold nanoparticles (AuNPs)-conjugated goat anti-human IgG (for SARS-CoV-2 IgG detection) and AuNPs-conjugated goat anti-human IgM (for SARS-CoV-2 IgM detection) were immobilized on the conjugated pad. The spike protein of SARS-CoV-2 (100 μg/mL) was dispensed on the nitrocellulose membrane as a test line (T) for both IgG and IgM detection. For the control line (C), the rabbit anti-goat IgG and rabbit anti-goat IgM (100 μg/mL) were also dispensed on the

nitrocellulose for SARS-CoV-2 IgG and IgM detection, respectively. The test strip was allowed to dry in an oven at 37°C for 1 hr. Lastly, the prepared LFA device was placed into a plastic housing and kept in a humidity-controlled box until use.

**The LFA detection principle and procedure**

For detection, 20 µL of the working standard/sample was added to the sample pad. Then, 80 µL of the tris running buffer was applied to the sample pad to enable the liquid transfer toward the absorbent pad. In this reaction, the targeted SARS-CoV-2 antibodies will capture with the deposited goat anti-human IgG/IgM–AuNPs on the conjugate pad. Next, these immunocomplexes between SARS-CoV-2 antibodies and goat anti-human IgG/IgM–AuNPs will be caught by the SP RBD at the T line, forming (goat anti-human IgG/IgM–AuNPs) – (SARS-CoV-2 antibodies) – (SP RBD of SARS-CoV-2) sandwiched complexes. In the meantime, the rabbit anti-goat IgG/IgM at the C line will also capture the goat anti-human IgG/IgM–AuNPs, forming (goat anti-human IgG/IgM–AuNPs) – (rabbit anti-goat IgG/IgM) complex. In the presence of the target SARS-CoV-2 antibodies, the reddish/purple color of AuNPs will appear on both lines. After the reaction was completed, the image processing was then used to interpret the color result in R color of RGB mode.

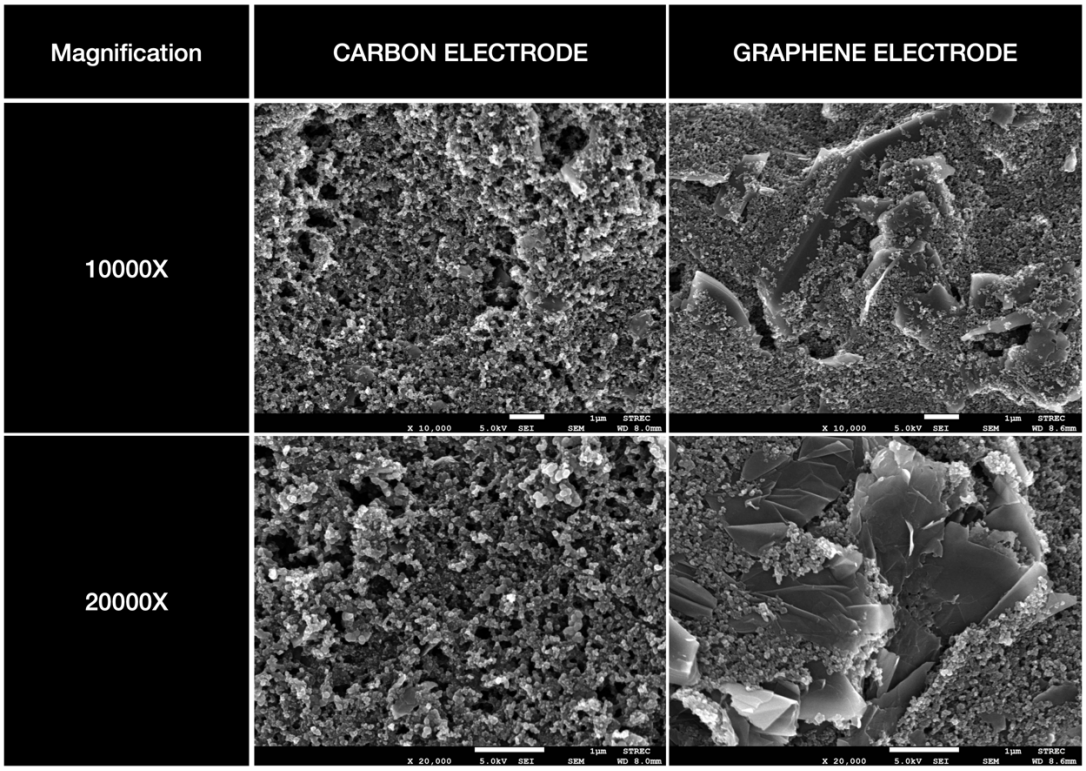


**Figure S1**. SEM images of the rear graphene electrode (right) compared to the carbon electrode (left) at different magnifications (10000X and 20000X).

Aside from the morphologies of bare paper and GO-modified electrode, we have further characterized the morphologies of the rear graphene electrode compared to the carbon electrode using SEM technique. Apparently in SEM images, the sensitive electrochemical response could be ascribed to the presence of graphene sheets (smooth flake) in the carbon/graphene paste (compared to that of carbon electrode).

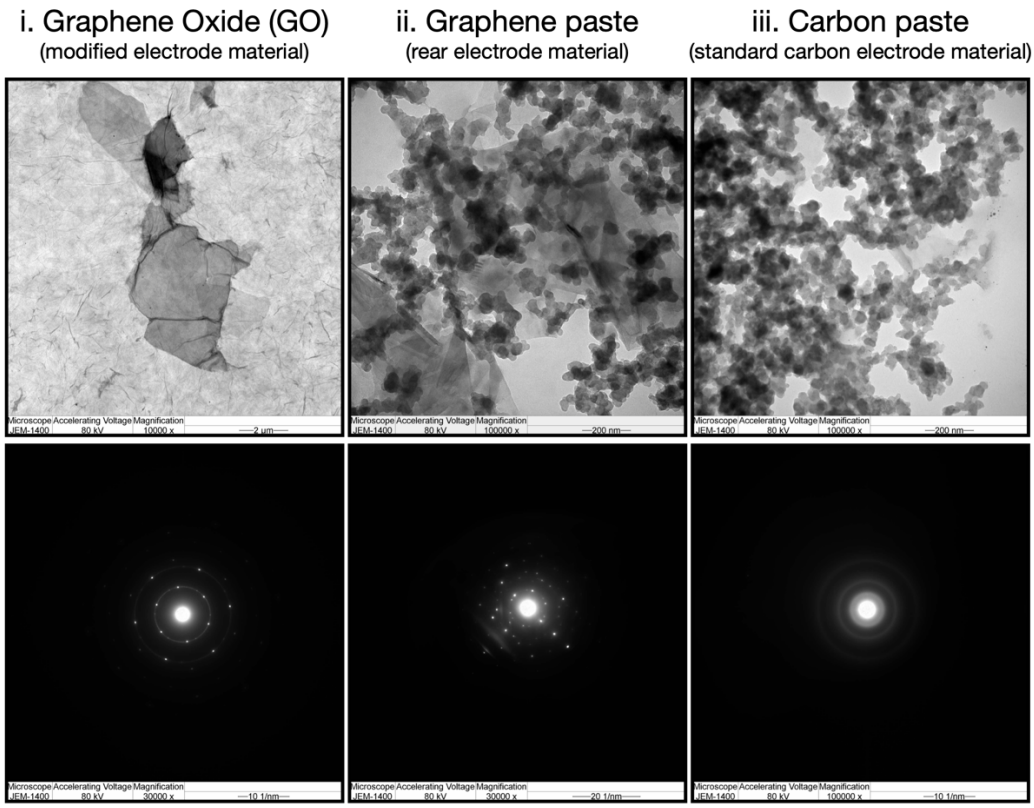


**Figure S2**. TEM images (upper) and their corresponding diffraction pattern (lower) of the electrode materials utilized in this work; graphene oxide (GO, i) and graphene paste (ii), compared to the standard carbon paste (iii).

Furthermore, we have characterized the morphologies of the electrode materials utilized in this work (including graphene oxide (GO) and rear graphene paste) compared to the standard carbon paste materials with the TEM technique. As illustrated in **Figure S2**, the graphene oxide (GO) solution used to embed on the bare paper electrode clearly showed the crumple flakes of the graphene sheet (i). Also, its corresponding hexagonal diffraction pattern clearly confirms the graphene-like carbon backbone. Likewise, the graphene paste material used as a rear electrode in this study exhibited a mixed nature of graphene flakes and amorphous carbon (ii). This image result is in line with the SEM image of the graphene electrode, in which graphene sheets were mixed with the carbon. Besides, the diffraction pattern of the graphene paste

material clearly exhibited a superimposed pattern of hexagonal graphene and amorphous carbon. We further compared these morphological results with that of the standard carbon paste material. In panel (iii), the carbon paste showed an aggregated carbon particle with a nature diffraction pattern of amorphous material.

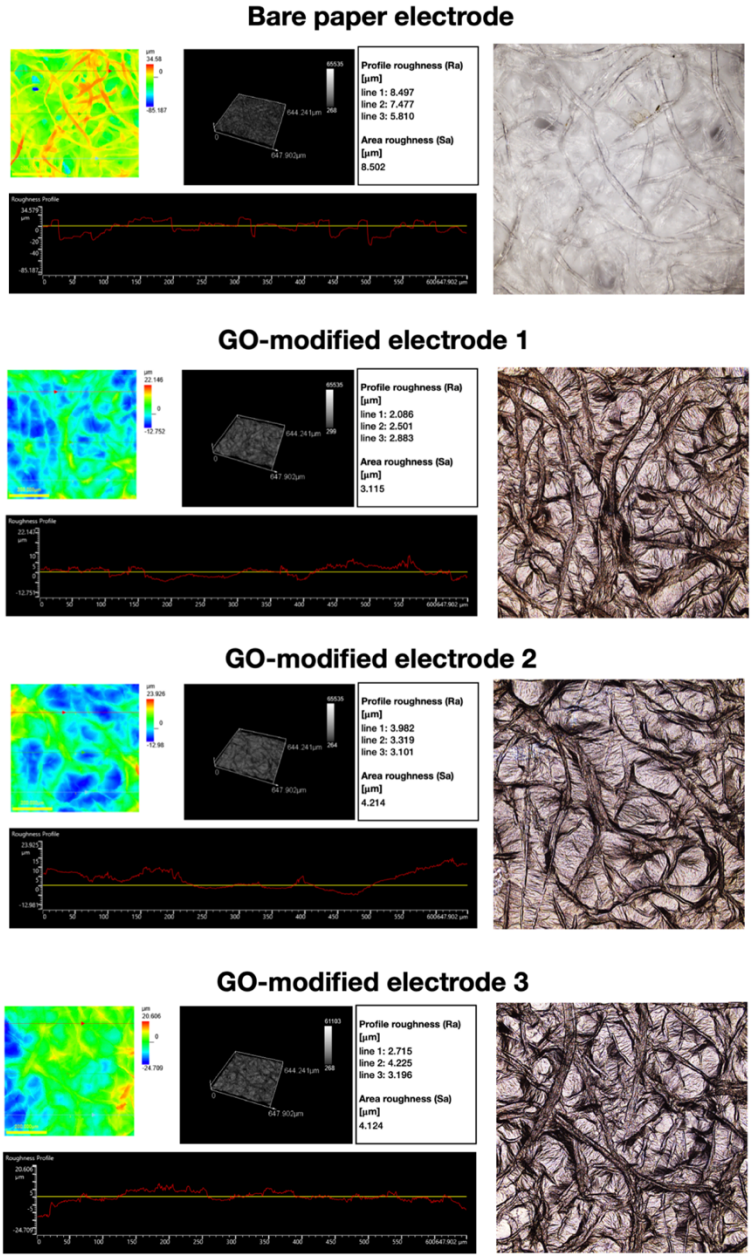


**Figure S3**. Confocal laser scanning microscopy images of the bare paper electrode and GO-modified electrode (n=3).

we have further characterized the difference in the shape of different electrodes (n=3) by laser scanning confocal microscopy (LSCM). This technique provides a helpful information regarding the 3D profile roughness (Ra) and area roughness (Sa) of samples as the electrode

surface is an important factor which further affects the electrochemical property. As shown in figure S3, the bare paper electrode provides an average profile roughness (Ra) of 7.261 $\mu$m while the GO-modified electrode showed a smoother surface with an average Ra of 3.112 $\mu$m. The standard deviation of the measured Ra from three different electrodes was found as low as 0.678. For the area roughness (Sa), the bare paper electrode provides an average Sa of 5.810 $\mu$m while the GO-modified electrode showed a lower area with an average Sa of 3.818 $\mu$m. The standard deviation of the measured Sa from three different electrodes was found to be 0.61. From these observed results, it can be concluded that there is no significant different between each modified electrode.

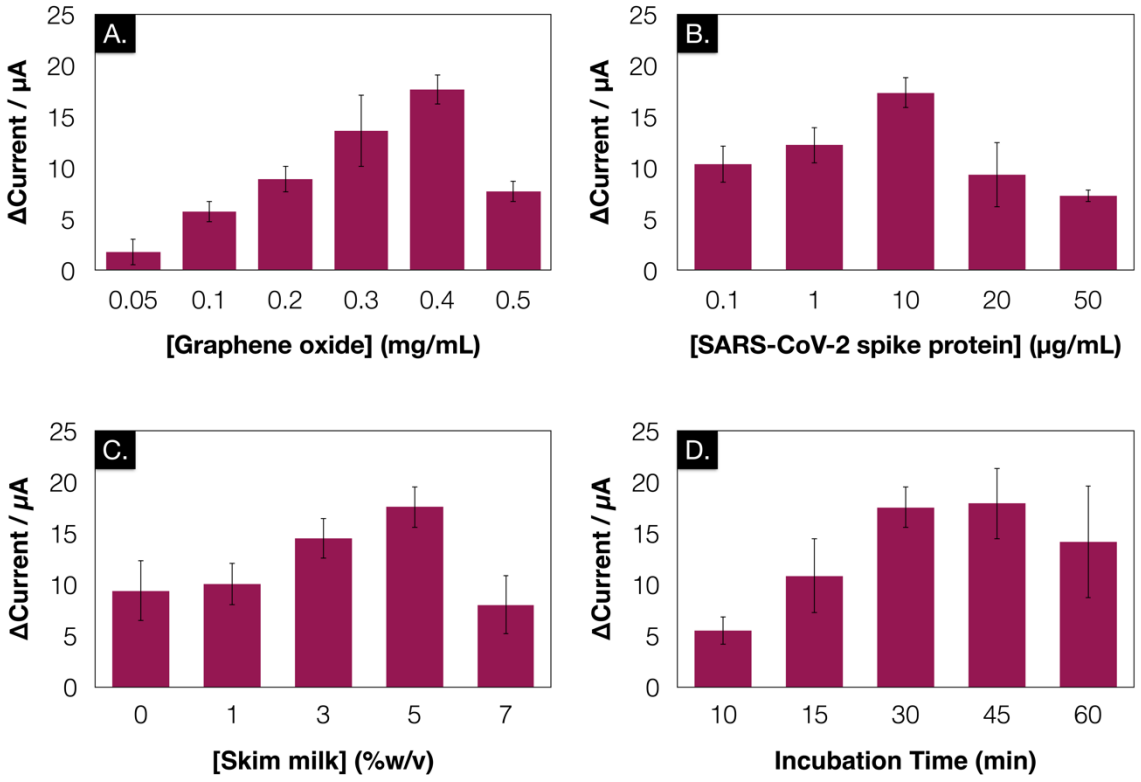


**Figure S4.** Effects of (A) graphene oxide concentration (mg/mL), (B) concentration of SARS-CoV-2 spike protein (μg/mL), (C) concentration of skim milk (% w/v), and (D) incubation time, on the label-free electrochemical detection of 1000 ng/mL SARS-CoV-2 IgG (n = 3).

**Assay Optimization**

In this present work, several parameters impacting the performance of COVID-19 ePAD (including GO concentration, SP RBD concentration, SKI concentration and incubation time) were studied to obtain the maximum sensing efficiency (**Figure S4**). Noted that a plotted signal (y-axis) was calculated from the difference of current (Δcurrent) between the absence (control) and presence of the IgG model antibody. We first studied the effect of GO concentration in the range of 0.05 to 0.5 mg/mL. It was observed in **Figure S4A** that the higher concentration of the GO yields in a higher Δcurrent due to an increase of specific oxygen-containing functionalities (−COOH immobilization sites), thus increasing the amount of an

immobilized SP RBD. However, excessive concentration of GO could also result in a poor electron transfer, which reduces the current response. Hence, GO concentration of 0.4 mg/mL was selected as it offers the highest sensitivity. Next, the effective concentration of an immobilized spike protein (SP-RBD) was optimized in the range of 0.1 to 50 µg/mL. It is evident in **Figure S4B** that the notable response was obtained at SP RBD concentration of 10 µg/mL. The amount of SP RBD exceeding this level is prone to reduce the electron transfer of $[Fe\ (CN)_6]^{3-/4-}$. Also, the percentage of blocking agent concentration was carefully selected based on the most sensitive response. Here, skim milk (SKI) was utilized as a blocking agent in this study due to its predominance of low molecular weight protein, which theoretically would have a more significant opportunity to fill in small areas between the larger immobilized protein (Diamandis and Christopoulos 1996). As displayed in **Figure S4C**, the most appropriate SKI concentration is 5% (w/v). In addition, the incubation time for the immunoreaction between SP RBD and targeted antibodies was studied in the range from 10 to 60 mins (**Figure S4D**). An optimum period of 30 min was chosen in this assay as it reached maximum response and remained steady at that period.

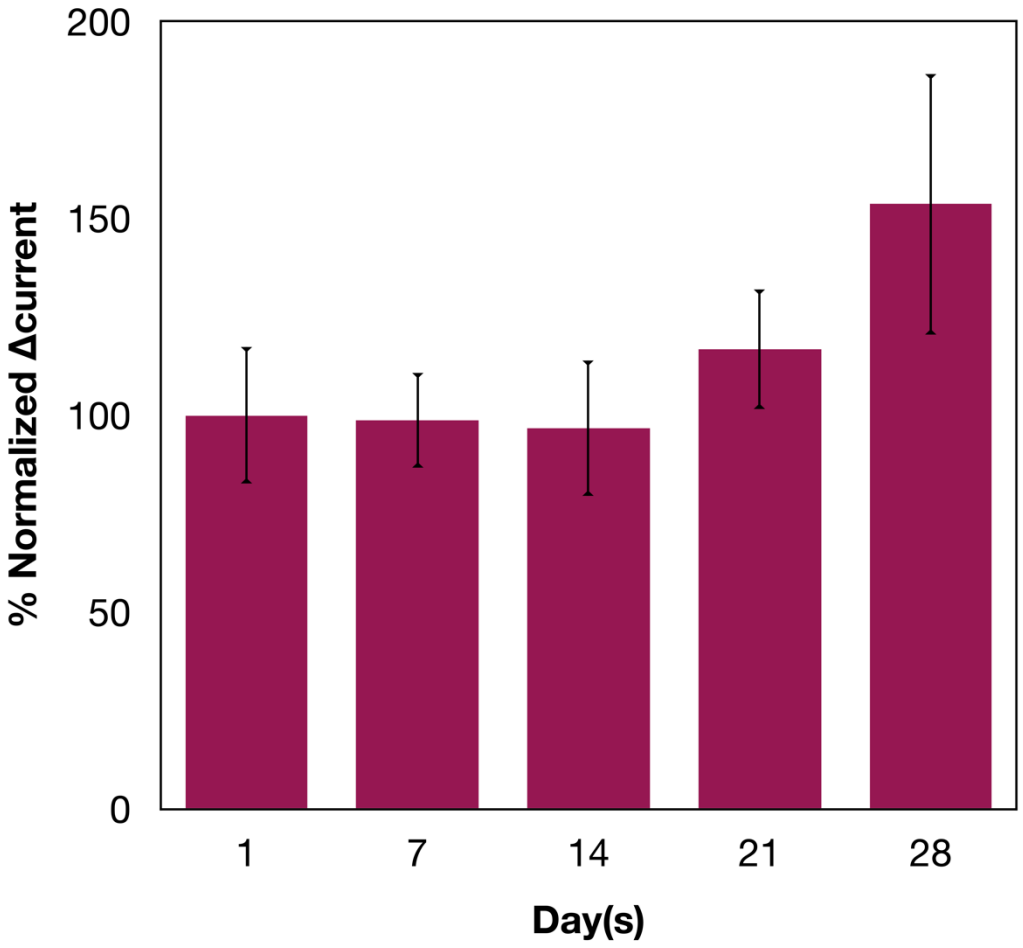


**Figure S5.** Stability of the COVID-19 ePAD serological assay tested with 1000 ng/mL SARS-CoV-2 IgG.

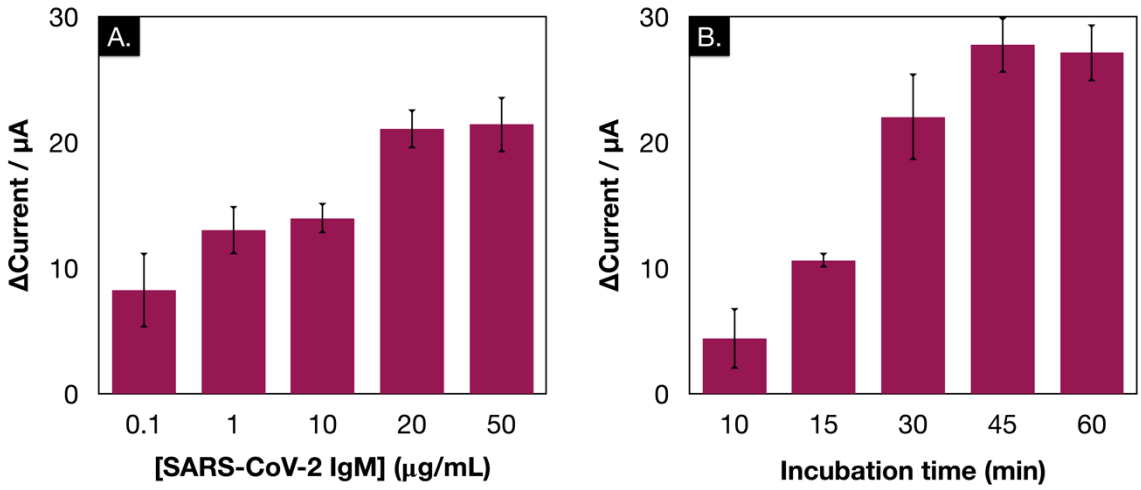


**Figure S6.** Effects of (A) SARS-CoV-2 IgM (μg/mL) and (B) incubation time on the label-free electrochemical detection of 1000 ng/mL SARS-CoV-2 spike protein (n = 3).

**Table S1.** Comparison of the analytical performance of other SARS-CoV-2 antibodies sensors with the proposed ePAD.

| Detection Platform | Targeting antibody | Labeling agent | Requirement of multiple antibodies | Detection limit | Linear dynamic range | Ref |
|---|---|---|---|---|---|---|
| Colorimetric LFA | IgM | Colloidal gold nanoparticle | ✓ | NA | NA | (Huang et al. 2020) |
| Colorimetric LFA | IgG | Colloidal gold nanoparticle | ✓ | NA | NA | (Wen et al. 2020) |
| Fluorescent LFA | IgG | Lanthanide-doped nanoparticle | ✓ | NA | NA | (Chen et al. 2020) |
| Gel card Agglutination assay | IgG | - | - | NA | NA | (Alves et al. 2020) |
| Electrochemical detection | IgG and IgM | - | - | 1 ng/mL for each antibody | 1 to 1000 ng/mL | This work |

LFA: lateral flow immunoassay, NA: no available, -: not required, ✓: required.

**Table S2.** Cross-reactivity study report using the proposed COVID-19 ePAD and commercial ELISA technique.

| Reactive serum samples | COVID-19 ePAD | Commercial ELISA |
|---|---|---|
| Anti-HBsAg | - | - |
| Anti-HCV | - | - |
| Anti EBV (IgG/IgM) / Anti Rubella (IgG) | - | - |
| Anti CMV (IgG/IgM) | - | - |

ELISA: Enzyme-linked immunosorbent assay, HCV: Hepatitis-C virus, HBsAg: Hepatitis B surface antigen, EBV: Epstein Barr virus, CMV: Cytomegalovirus, -: negative result.

## References

Alves, D., Curvello, R., Henderson, E., Kesarwani, V., Walker, J.A., Leguizamon, S.C., McLiesh, H., Raghuwanshi, V.S., Samadian, H., Wood, E.M., McQuilten, Z.K., Graham, M., Wieringa, M., Korman, T.M., Scott, T.F., Banaszak Holl, M.M., Garnier, G., Corrie, S.R., 2020. Rapid Gel Card Agglutination Assays for Serological Analysis Following SARS-CoV-2 Infection in Humans. ACS Sensors 5(8), 2596-2603.

Chen, Z., Zhang, Z., Zhai, X., Li, Y., Lin, L., Zhao, H., Bian, L., Li, P., Yu, L., Wu, Y., Lin, G., 2020. Rapid and Sensitive Detection of anti-SARS-CoV-2 IgG, Using Lanthanide-Doped Nanoparticles-Based Lateral Flow Immunoassay. Analytical Chemistry 92(10), 7226-7231.

Diamandis, E.P., Christopoulos, T.K., 1996. Immunoassay. Elsevier Science.

Huang, C., Wen, T., Shi, F.-J., Zeng, X.-Y., Jiao, Y.-J., 2020. Rapid Detection of IgM Antibodies against the SARS-CoV-2 Virus via Colloidal Gold Nanoparticle-Based Lateral-Flow Assay. ACS Omega 5(21), 12550-12556.

Wen, T., Huang, C., Shi, F.-J., Zeng, X.-Y., Lu, T., Ding, S.-N., Jiao, Y.-J., 2020. Development of a lateral flow immunoassay strip for rapid detection of IgG antibody against SARS-CoV-2 virus. Analyst 145(15), 5345-5352.

Zhang, G., Guo, J., Wang, X., 2009. Immunochromatographic Lateral Flow Strip Tests. In: Rasooly, A., Herold, K.E. (Eds.), Biosensors and Biodetection: Methods and Protocols: Electrochemical and Mechanical Detectors, Lateral Flow and Ligands for Biosensors, pp. 169-183. Humana Press, Totowa, NJ.